ingly, the indices of refraction), were obtained from least squares fitting of the reflectivity (*29*) [see the vertical and horizontal 1:2 (reflectivity) scans in Fig. 3].
19. $k_{y,intern}$ is given by $k^2 = n^2(2\pi/\lambda)^2 = k_{x,intern}^2 + k_{y,intern}^2 + k_{z,intern}^2$, where $k_{x,intern} = nk\ \sin(\phi_{i,intern})$ and $k_{z,intern} = nk\ \sin(\alpha_{i,intern})$.
20. A. K. Ghatak, K. Thyagarajan, *Introduction to Fiber Optics* (Cambridge Univ. Press, Cambridge, 1998).
21. This case corresponds to the radiation modes or leaky modes of a waveguide and will not be discussed here (*14*, *19*).
22. The cutoff angle is obtained from $\alpha_{c,intern} = (\alpha_{c,cladding}^2 - \alpha_{c,core}^2)^{1/2}$, with a critical angle of $\alpha_c = (2\delta)^{1/2}$. With the above values, an internal cutoff angle of $\alpha_{c,internal} = 0.203°$ is obtained. Therefore, the guide supports seven resonance orders in the *x* direction (ϕ_{intern}) and three resonance orders in the *z* direction (α_{intern}).
23. The FWHM of the Ψ^{11} field intensity distribution in the waveguides guiding channel is 68.7 nm in the *x* direction and 33.0 nm in the *z* direction.
24. Photons can exit the guide at the end (rear face) if the footprint of the beam is separated from the end no farther than the so-called coupling length (in our case, ~750 μm).
25. Materials and methods are available as supporting material on *Science* Online.
26. The results shown here were obtained at the ID13 and ID01 beamlines (at the European Synchrotron Radiation Facility), with slightly different wavelengths but at comparable beam dimension and beam characteristics. In order to compare the results, the additional data set was rescaled to match the wavelength $\lambda = 0.097$ nm of the main experiment.
27. Standard reflectivity from thin-film layers is carried out by measuring the reflected intensity as a function of the angle on incidence, at $\alpha_i = \alpha_f$ and $\phi_i = \phi_f = 0$.
28. This nonstandard type of reflectivity, described in detail elsewhere, uses the fact that single, line-like nanostructures give rise to a circular diffraction pattern, subject to the constraint $q_y = 0$ ($\alpha_i^2 + \phi_i^2 = \alpha_f^2 + \phi_f^2$). Thus, by measuring the reflectivity in ϕ_i and ϕ_f at a fixed, small offset in α_i/α_f ($\alpha_i = \alpha_f \cong 0.05°$ was used in the present case), the lateral geometry (in the *x* direction) of the nanostructure can be probed. Values for the width *w* could thus be determined for several devices (a representative measurement and the corresponding fit are shown in Fig. 3A). Importantly, this circular diffraction pattern centered around the axis of the capillary observed for all angles may not be confused with the resonance effects.
29. L. G. Parratt, *Phys. Rev.* **95**, 359 (1954).
30. The mapping in Fig. 2D was obtained by modifying the refraction-corrected solution, displayed in Fig. 2B, according to the following equation:

$$I(\phi_i,\alpha_i) = \sum_{p,q} \exp\left(\frac{(\phi_i - \phi_i^p)^2}{2\sigma_{\phi i}^2}\right) \exp\left(\frac{(\alpha_i - \alpha_i^p)^2}{2\sigma_{\alpha i}^2}\right) \exp\left(\frac{(\phi_i^2 + \alpha_i^2) - ((\sigma_i^{p2}) + (\alpha_i^q))^2}{2\sigma_{radial}^2}\right) \quad (3)$$

with $\sigma_{\phi i} = 0.015°$, $\sigma_{\alpha i} = 0.01°$, and $\sigma_{radial} = 0.0011°$.
31. The rms roughness σ must not be small with respect to λ but with respect to λ/(sin α). In practice, total reflection can still occur up to about $\sigma \cong 1.5$ nm.
32. The measurements (not shown here) were carried out by scanning a 5-μm Ir/Pt pinhole (SPI, West Chester, PA) along the *x* and *z* directions on a piezo stage (Piezosystem Jena, Jena, Germany) at a distance of ≅1.0 mm behind the guide, confirming the exit beam divergence and thus also the conclusion that the exit beam originates from the end of the guide (waveguide point source).
33. This number exceeds the flux through a hypothetical pinhole of equivalent size by a factor of about 70. Improved fabrication can be expected to increase the output flux and hence the gain by orders of magnitude, similar to the recent progress in planar waveguides.

34. We thank H. Metzger for providing the additional time at beamline ID1 necessary to complement the ID13 data, as well as D. Le Belloc'h and A. Mazuelas for help at ID1. We are indebted to J. Kotthaus, H. Gaub, and J. Peisl at the Center for NanoScience Munich for advice and encouragement to carry out this project. We gratefully acknowledge financial support by Deutsche Forschungsgemeinschaft SFB-486.

Supporting Online Material
www.sciencemag.org/cgi/content/full/297/5579/230/DC1
Materials and Methods
Fig. S1
Table S1

19 March 2002; accepted 31 May 2002

Spin-Polarized Resonant Tunneling in Magnetic Tunnel Junctions

S. Yuasa,* T. Nagahama, Y. Suzuki

Insertion of a thin nonmagnetic copper Cu(001) layer between the tunnel barrier and the ferromagnetic electrode of a magnetic tunnel junction is shown to result in the oscillation of the tunnel magnetoresistance as a function of the Cu layer thickness. The effect is interpreted in terms of the formation of spin-polarized resonant tunneling. The amplitude of the oscillation is so large that even the sign of the tunnel magnetoresistance alternates. The oscillation period depends on the applied bias voltage, reflecting the energy band structure of Cu. The results are encouraging for the development of spin-dependent resonant tunneling devices.

A new field of electronics called spin electronics (*1, 2*), which makes use of both the electric charge and the spin of conduction electrons, has been developing rapidly in systems such as metallic magnetic multilayers, magnetic semiconductors, and strongly correlated electron systems. Among these systems, a magnetic tunnel junction (MTJ), which consists of two ferromagnetic (FM) metal layers (electrodes) separated by a thin insulating layer (tunnel barrier) and shows the tunnel magnetoresistance (TMR) effect (*3–5*), is especially important for application to magnetoresistive random-access memory (MRAM) devices. Highly functional spin-electronic devices such as spin transistors cannot be realized without a better understanding of the mechanism of spin-polarized electron transport, because it is still unclear how the coherence of the wave functions and spins of the conduction electrons are conserved in the transport process. For example, the resonant-tunneling effect (i.e., coherent tunneling of electrons from one electrode to the other through quantum well states formed between the two electrodes) (*6*), in which the coherence of electron wave functions is essential, has never been well controlled in spin-polarized systems such as MTJs and magnetic semiconductors. Spin-polarized resonant tunneling is crucial for the development of highly functional devices, such as a resonant-tunneling spin transistor (*7*) and quantum information devices, because the coherency of both the wave functions and the spins of conduction electrons should be conserved in those devices.

One of the simplest ways to realize spin-polarized resonant tunneling is to insert a nonmagnetic (NM) metal layer between the insulating tunnel barrier (I) and one of the two FM electrodes in a MTJ. Because spin-dependent reflections of the conduction electrons take place at the FM-NM interface (Fig. 1A), spin-polarized quantum well (QW) states are created in the NM layer (*8, 9*) and spin-polarized tunneling electrons will resonantly pass through the NM layer. Theories predict an oscillation of the TMR effect as a function of the NM layer thickness because the spin polarization of the tunneling electrons oscillates as a result of the resonant tunneling (*10, 11*). Although a number of experimental studies have been made, there have been no reports of an oscillation being observed (*12–17*). To date, the TMR ratio has usually been found to decrease monotonically with NM layer thickness (*12*). Moodera *et al*., using a NM Au layer (polycrystalline), first observed a sign reversal of the TMR ratio (*13*). Although it was attributed to a quantum size effect, no oscillation of the TMR was observed. LeClair used a NM Ru layer and obtained a similar result (*17*). The sign reversal of TMR was, however, attributed to a change of the density of states (DOS) of the electrode due to the interfacial mixing, not due to the quantum size effect. It was also found that the TMR effect almost disappears at a NM layer thickness of about 6 Å (*13–17*), indicating that the

NanoElectronics Research Institute, National Institute of Advanced Industrial Science and Technology, Tsukuba 305-8568, Japan, and Core Research for Evolutional Science and Technology, Japan Science and Technology Corporation, 4-1-8 Honcho, Kawaguchi 332-0012, Japan.

*To whom correspondence should be addressed. E-mail: yuasa-s@aist.go.jp

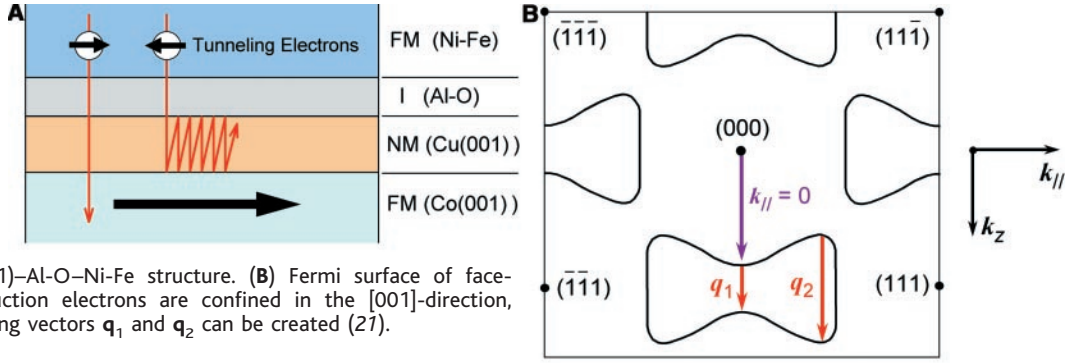

Fig. 1. (**A**) Schematic diagram of the magnetic tunnel junction (MTJ) with FM-NM-I-FM structure, in which electrons with different spin directions tunnel from the upper to the bottom electrodes. FM, NM, and I denote a ferromagnetic electrode, a nonmagnetic layer, and an insulating layer (tunnel barrier), respectively. We prepared the MTJs to have a Co(001)–Cu(001)–Al-O–Ni-Fe structure. (**B**) Fermi surface of face-centered cubic Cu. When conduction electrons are confined in the [001]-direction, quantum-well states with scattering vectors $\mathbf{q}_1$ and $\mathbf{q}_2$ can be created (*21*).

spin polarization of a tunneling electron is completely scattered when it passes through the 6 Å NM layer. Such a short spin scattering length will prevent spin-polarized resonant tunneling. However, the strong spin scattering seems to be attributable to the polycrystalline nature of the samples. The MTJs with a single-crystal electrode will be indispensable for spin-polarized resonant tunneling.

In our previous study, we prepared a MTJ with an ultrathin FM Fe(001) single-crystal electrode and observed a small oscillation of TMR as a function of the bias voltage (*18*). In this case, however, the resonant tunneling is not necessary for the oscillation of TMR because an incoherent tunneling to the ultrathin Fe electrode, in which the spin polarization is modulated by QW states, can result in the oscillation of TMR. Moreover, the quantum-well effect is very small because of the short mean free path and spin diffusion length in the FM metal, and therefore a theoretical analysis is difficult to perform (*18*). On the contrary, in the MTJs with a NM insertion layer, the resonant tunneling through the NM layer is essential for the TMR oscillation. A single-crystal layer made of a NM noble metal is ideal for the resonant tunneling because of the long mean free path. We report that a clear spin-polarized resonant tunneling is realized by using a single-crystal electrode made of a NM Cu(001) layer grown on Co(001).

The MTJs, Co(001)–Cu(001)–Al-O–Ni-Fe (Fig. 1A), were prepared by using a molecular beam epitaxy technique and the subsequent microfabrication processes (*19*). The thickness of the Cu(001) layer, t_{Cu}, was changed from zero to 29 Å in order to study the t_{Cu} dependence of the TMR effect. MTJs were prepared with thicknesses of the Al-O tunnel barrier $t_{Al\text{-}O}$ = 12, 18, and 24 Å; the size of the junctions was 2 μm by 2 μm (*20*). The electric resistance was measured by the dc four-probe method with a bias voltage up to 700 mV. The bias voltage direction was defined with respect to the Co-Cu electrode. Magnetoresistance measurements were carried out at 2 K and 300 K in magnetic fields up to 2 T. In addition to the MTJs, we also prepared Co(001)-Cu(001)-Co(001) films (t_{Cu} = 0 to 40 Å) using the same substrate and buffer layers (*20*) and investigated the interlayer exchange coupling through the Cu(001) layer. It is known that the interlayer exchange coupling oscillates as a function of the Cu layer thickness because of the QW states formed at the Fermi level in Cu (*21*).

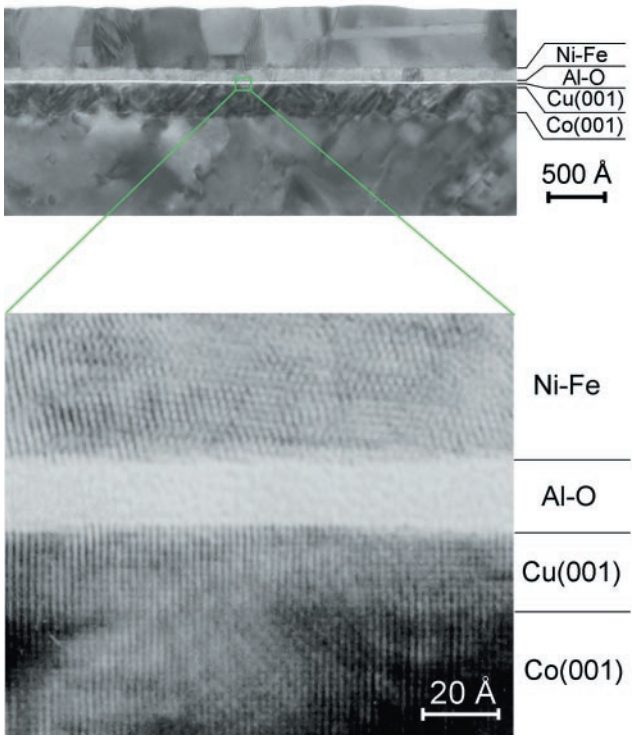

Fig. 2. High-resolution TEM images of a tunnel junction with a Co(001) (200 Å)–Cu(001) (20 Å)–Al-O (18 Å)–$Ni_{80}Fe_{20}$ (100 Å) structure.

In the transmission electron microscope (TEM) image of a tunnel junction with a Co(001)–Cu(001) (20 Å)–Al-O (18 Å)–Ni-Fe structure (Fig. 2), the bottom electrode [Co(001)-Cu(001) layer] is a single crystal, the Al-O tunnel barrier has an amorphous structure, and the upper electrode (Ni-Fe layer) is polycrystalline. A very flat Cu(001) layer with monoatomic steps on the interfaces was prepared. Typical magnetoresistance curves for t_{Cu} = 0 Å and 4.5 Å are shown in Fig. 3, A and B, respectively. The MTJ with t_{Cu} = 0 Å shows the usual positive TMR effect, whereas the MTJ with t_{Cu} = 4.5 Å shows an anomalous negative (inverse) TMR effect. The antiparallel magnetic configurations were well realized in both cases because of the different coercive forces (H_C) for the bottom electrode (Co) (H_C = 25 mT) and for the upper electrode (Ni-Fe) (H_C < 3 mT). This means that there is little magnetic coupling between the two electrodes.

Figure 3C shows the TMR ratio at temperatures of 2 K and 300 K at a low bias voltage (+10 mV) as a function of t_{Cu}. The TMR ratio is defined as $\Delta R/R_p = (R_a - R_p)/R_p$, where R_p and R_a are the tunnel resistance when the magnetizations of the two FM electrodes are aligned parallel and antiparallel, respectively. The TMR ratio clearly oscillates up to t_{Cu} = 29 Å. It is noteworthy that the amplitude of the TMR oscillation is so large that even the sign of the TMR ratio alternates. The TMR oscillation is well fitted to a damped oscillation function plus a small positive background curve (a simple damping curve). The origin of the background is not clear at the present stage. The period of the TMR oscillation is 11.4 Å. On the other

hand, the tunnel resistance (R_p) itself also shows a slight oscillatory behavior, although it is not as clear as the TMR oscillation. The tunnel resistance takes a maximum at t_{Cu} = 4.5 Å where the TMR ratio takes a minimum (negative) value. We carried out the same measurements on the MTJs with different Al-O thicknesses ($t_{Al\text{-}O}$ = 12, 18, or 24 Å) and obtained essentially the same results on the TMR oscillation while the tunnel resistance itself exponentially increased from 100 ohm·μm^2 ($t_{Al\text{-}O}$ = 12 Å) to 7 × 10^7 ohm·μm^2 ($t_{Al\text{-}O}$ = 24 Å).

As a possible origin of the TMR oscillation, we note that spin-dependent reflection of conduction electrons occurs at the Co-Cu interface (Fig. 1A). The tunneling electrons with up-spin (defined as a spin parallel to the magnetization of Co) easily transmit into the Co layer, whereas the tunneling electrons with down-spin (defined as a spin antiparallel to the magnetization of Co) have a higher probability to be reflected at the Co-Cu interface. If multiple scatterings occur between the Co-Cu and Cu–Al-O interfaces, the down-spin electrons form resonant states (QW states) in the Cu layer. Two kinds of QW states corresponding to the scattering vectors $\mathbf{q}_1$ and $\mathbf{q}_2$ are known to be formed in an ultrathin Cu(001) (Fig. 1B) (*21*). According to the band calculations, $\mathbf{q}_1$ and $\mathbf{q}_2$ are responsible for the QW oscillations with periods 10.6 Å and 5.9 Å, respectively (*21*). Such oscillations are observed in the interlayer exchange coupling through the Cu(001) layer, although the short-period oscillation due to $\mathbf{q}_2$ easily disappears because of the atomic-scale roughness of the films (*8, 21, 22*). The observed period of the TMR oscillation (11.4 Å) agrees (within experimental error) with the long-period oscillation due to $\mathbf{q}_1$. On the other hand, the interlayer exchange coupling in the Co(001)-Cu(001)-Co(001) films prepared in this study show a QW oscillation with a period of 11 Å (fig. S1), which is the same as the period of the TMR oscillation. Those agreements clearly suggest that both the TMR and the exchange coupling oscillations originate from the same QW states corresponding to $\mathbf{q}_1$ at the Fermi level. We successfully observed the QW oscillation of the TMR effect, although other researchers observed no oscillatory behavior with a polycrystalline Cu layer (*12, 14–16*). It is noted here that conduction electrons with a wave vector $\mathbf{k}$ normal to the tunnel barrier ($\mathbf{k}_{//}$ = 0) are the main contributors to the tunneling current in an ideal tunnel junction (*19, 23*). This is because the tunneling probability sharply decreases as the direction of $\mathbf{k}$ deviates from the barrier normal. Consequently, the tunneling electrons can be efficiently injected into the QW states located at $\mathbf{k}_{//}$ = 0 (i.e., the QW states of $\mathbf{q}_1$) (Fig. 1B).

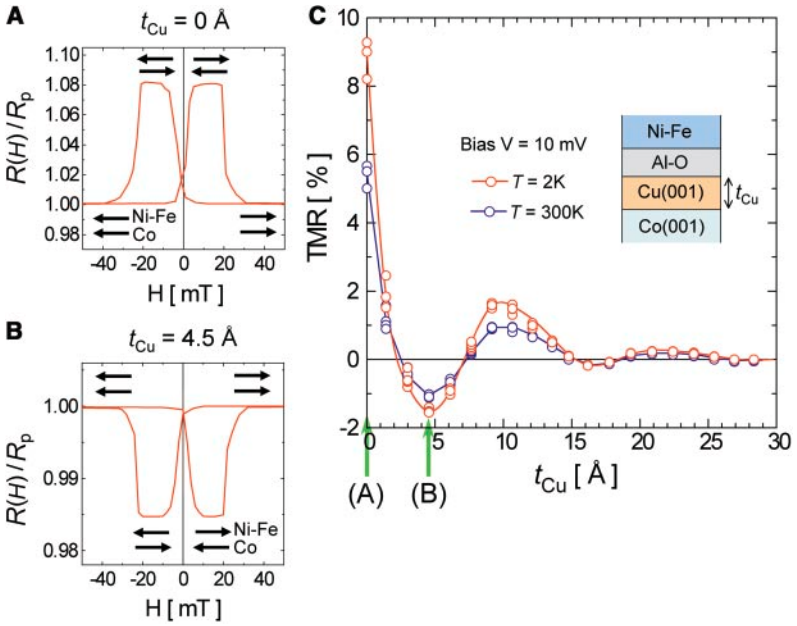

Fig. 3. Normalized TMR curves at T = 2 K at a bias voltage of +10 mV for Co(001)–Cu(001)–Al-O (18 Å)–$Ni_{80}Fe_{20}$ junctions with Cu layer thickness (t_{Cu}) of (**A**) 0 Å and (**B**) 4.5 Å. R_p denotes the tunnel resistance with parallel magnetization configuration. (**C**) TMR ratio at T = 2 K and 300 K at a bias voltage of +10 mV as a function of t_{Cu}.

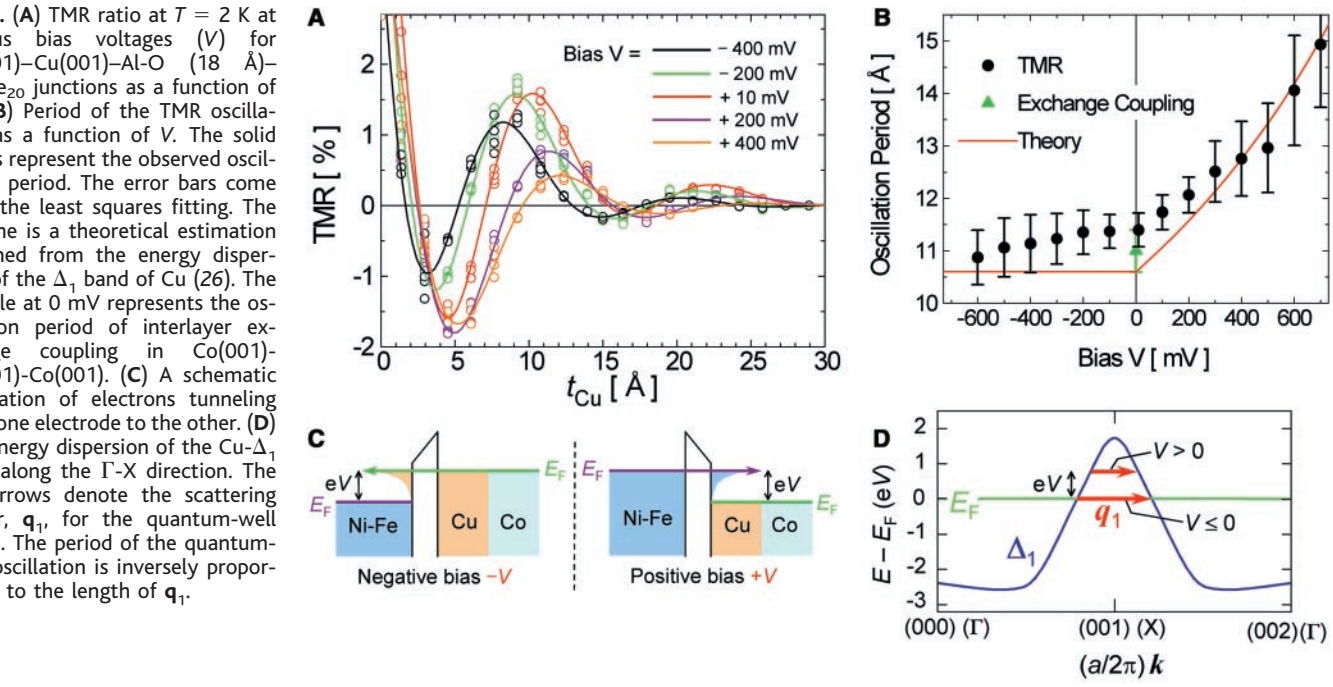

Fig. 4. (**A**) TMR ratio at T = 2 K at various bias voltages (V) for Co(001)–Cu(001)–Al-O (18 Å)–$Ni_{80}Fe_{20}$ junctions as a function of t_{Cu}. (**B**) Period of the TMR oscillation as a function of V. The solid circles represent the observed oscillation period. The error bars come from the least squares fitting. The red line is a theoretical estimation obtained from the energy dispersion of the Δ_1 band of Cu (*26*). The triangle at 0 mV represents the oscillation period of interlayer exchange coupling in Co(001)-Cu(001)-Co(001). (**C**) A schematic illustration of electrons tunneling from one electrode to the other. (**D**) The energy dispersion of the Cu-Δ_1 band along the Γ-X direction. The red arrows denote the scattering vector, $\mathbf{q}_1$, for the quantum-well states. The period of the quantum-well oscillation is inversely proportional to the length of $\mathbf{q}_1$.

For the origin of the anomalous negative TMR effect, the TMR ratio can be formulated in terms of the spin polarizations of electrodes (i.e., the difference between the DOS of up and down spin bands). According to Julliere's formulation (*24*), the TMR ratio at a low bias-voltage limit is expressed as

$$\mathrm{TMR} = (R_a - R_p)/R_p = 2PP'/(1 - PP') \quad (1)$$

where P and P' are the spin polarizations of the two electrodes. Because the spin polarization of Ni-Fe is positive (*25*), the negative TMR indicates that the spin polarization of the Co-Cu electrode is effectively switched by the resonant-tunneling effect. Standing waves of wave functions of the conduction electrons (i.e., the QW states) in Cu(001) are effectively formed under the condition $t_{Cu} \cdot q + \alpha_1 + \alpha_2 = 2\pi n$, where α_1 and α_2 are phase changes of the electron wave functions induced by the reflections at the Co-Cu and Cu–Al-O interfaces, respectively, and n is an integer number. The QW states are formed when $t_{Cu} = 2\pi n/q_1 +$ constant; therefore, the period of QW oscillation is $2\pi/q_1$. Because the down-spin electrons are mainly confined in the Cu layer, the QW states should have a negative spin polarization. Thus, the TMR effect may change sign with a periodicity of $2\pi/q_1 \approx 11$ Å.

The TMR oscillation at various bias voltages is shown in Fig. 4A. All the curves can be fitted by using the same damped oscillation function. The parameters (e.g., the oscillation period, phase, and amplitude) change depending on the bias voltage. Here we discuss only the oscillation period, whose physical origin is the most straightforward. Figure 4B shows the bias dependence of the oscillation period. Under a positive bias, the oscillation period increases with the bias voltage. Under a negative bias, on the other hand, the oscillation period is approximately independent of the bias voltage. The theoretical value of the oscillation period estimated from the band structure of Cu (*26*) is also shown in Fig. 4B. The overall shape of the observed bias dependence is well reproduced by the theoretical estimation. To obtain the theoretical curve, we assumed a simple picture in which ballistic electrons tunnel from one electrode into the other without energy loss (Fig. 4C). Under a positive bias ($+V$), electrons at the Fermi level (E_F) in Ni-Fe dominantly tunnel into the empty states at $E_F + eV$ in Cu. In this case, the QW states at $E_F + eV$ in Cu have a strong influence on the TMR effect. Therefore, the oscillation period is determined by the length of the $\mathbf{q}_1$ vector at $E_F + eV$. Thus, the period is expected to depend on the bias voltage, reflecting the energy dependence of q_1 (i.e., the energy dispersion of the Δ_1 band of Cu along the Γ-X axis) (Fig. 4D) (*26*). Under a negative bias ($-V$), on the other hand, electrons at E_F in Cu dominantly tunnel into the empty states at $E_F + eV$ in Ni-Fe. In this case, the QW states at E_F in Cu have a strong influence on the TMR effect. Therefore, the oscillation period is expected to be independent of the bias voltage. The observed period at zero bias is slightly longer than the theoretical value. This discrepancy is also observed in the interlayer exchange coupling, where the observed oscillation period (*27*) is usually longer than the theoretical estimation (*21*). Although the theoretical estimation is based on an assumption that the tunneling process is ballistic (without energy loss), the observed TMR oscillation can be well explained by the theory.

We have shown that the coherence of spin-polarized tunneling electrons can be conserved after multiple reflections in the electrode, resulting in the spin-polarized resonant tunneling. With the use of this effect, it is possible to develop highly functional spin-electronic devices based on coherent transport, such as the resonant-tunneling spin transistor and quantum information devices.

References and Notes

1. G. A. Prinz, *Science* **282**, 1660 (1998).
2. S. A. Wolf *et al.*, *Science* **294**, 1488 (2001).
3. J. S. Moodera, L. R. Kinder, T. M. Wong, R. Meservey, *Phys. Rev. Lett.* **74**, 3273 (1995).
4. T. Miyazaki, N. Tezuka, *J. Magn. Magn. Mater.* **139**, L231 (1995).
5. J. M. de Teresa *et al.*, *Science* **286**, 507 (1999).
6. L. Esaki, *IEEE J. Quantum Electron.* **22**, 1611 (1986).
7. X. Zhan, B. Li, G. Sun, F. Pu, *Phys. Rev. B* **56**, 5484 (1997).
8. J. E. Ortega, F. J. Himpsel, G. J. Mankey, R. F. Willis, *Phys. Rev. B* **47**, 1540 (1993).
9. Y. Suzuki *et al.*, *Phys. Rev. Lett.* **80**, 5200 (1998).
10. A. Vedyayev, N. Ryzhanova, C. Lacroix, L. Giacomoni, B. Dieny, *Europhys. Lett.* **39**, 219 (1997).
11. J. Mathon, A. Umerski, *Phys. Rev. B* **60**, 1117 (1999).
12. J. J. Sun, P. P. Freitas, *J. Appl. Phys.* **85**, 5264 (1999).
13. J. S. Moodera *et al.*, *Phys. Rev. Lett.* **83**, 3029 (1999).
14. P. LeClair, H. J. M. Swagten, J. T. Kohlhepp, R. J. M. van de Veedonk, W. J. M. de Jonge, *Phys. Rev. Lett.* **84**, 2933 (2000).
15. J. S. Moodera, T. H. Kim, C. Tanaka, C. H. de Groot, *Philos. Mag. B* **80**, 195 (2000).
16. P. LeClair, J. T. Kohlhepp, H. J. M. Swagten, W. J. M. de Jonge, *Phys. Rev. Lett.* **86**, 1066 (2001).
17. P. LeClair *et al.*, *Phys. Rev. B* **64**, 100406-1 (2001).
18. T. Nagahama, S. Yuasa, Y. Suzuki, E. Tamura, *Appl. Phys. Lett.* **79**, 4381 (2001).
19. S. Yuasa *et al.*, *Europhys. Lett.* **52**, 344 (2000).
20. See supporting data on *Science* Online.
21. P. Bruno, C. Chappert, *Phys. Rev. Lett.* **67**, 1602 (1991).
22. A. Cebollada *et al.*, *Phys. Rev. B* **39**, 9726 (1989).
23. C. B. Duke, *Tunneling in Solids* (Academic Press, New York, 1969), chap. IV.
24. M. Julliere, *Phys. Lett.* **54A**, 225 (1975).
25. R. Meservy, P. M. Tedrow, *Phys. Rep.* **238**, 173 (1994).
26. B. Segall, *Phys. Rev.* **125**, 109 (1962).
27. W. Weber, R. Allenspach, A. Bischof, *Europhys. Lett.* **31**, 491 (1995).

Supporting Online Material

www.sciencemag.org/cgi/content/full/297/5579/234/DC1
Materials and Methods
Fig. S1

26 February 2002; accepted 13 May 2002

Spontaneous Organization of Single CdTe Nanoparticles into Luminescent Nanowires

Zhiyong Tang,[1] Nicholas A. Kotov,[1]* Michael Giersig[2]

Nanoparticles of CdTe were found to spontaneously reorganize into crystalline nanowires upon controlled removal of the protective shell of organic stabilizer. The intermediate step in the nanowire formation was found to be pearl-necklace aggregates. Strong dipole-dipole interaction is believed to be the driving force of nanoparticle self-organization. The linear aggregates subsequently recrystallized into nanowires whose diameter was determined by the diameter of the nanoparticles. The produced nanowires have high aspect ratio, uniformity, and optical activity. These findings demonstrate the collective behavior of nanoparticles as well as a convenient, simple technique for production of one-dimensional semiconductor colloids suitable for subsequent processing into quantum-confined superstructures, materials, and devices.

Unique structure and optical and electrical properties of one-dimensional (1D) semiconductors and metals make them the key structural blocks for a new generation of electronics, sensors, and photonics materials. Several synthetic methods of nanowire and nanorod production have been developed (*1–8*), but they all are based on point-initiated uniaxial growth of the crystal. Lateral expansion of the crystal lattice is arrested by a rigid template or by unfavorable kinetics. We describe a method of nanowire synthesis based on a different principle—a crystalline nanowire spontaneously self-assembles from individual nanoparticles. This technique of nanowire

[1]Chemistry Department, Oklahoma State University, Stillwater, OK 74078, USA. [2]Hahn-Meitner-Institut, Abteilung Physikalische Chemie Glienickerstrasse 100, D-15109, Berlin, Germany.

*To whom correspondence should be addressed. E-mail: kotov@okstate.edu